View metadata, citation and similar papers at core.ac.uk

brought to you by CORE

provided by DSpace@MIT

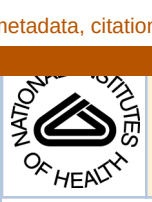

NIH Public Access

Author Manuscript

Cancer Res. Author manuscript; available in PMC 2012 September 1.

Published in final edited form as:

Cancer Res. 2011 September 1; 71(17): 5850–5858. doi:10.1158/0008-5472.CAN-11-1014.

BCL-2 family genetic profiling reveals microenvironment-specific determinants of chemotherapeutic response

Justin R. Pritchard[1,*], **Luke A. Gilbert**[1,*], **Corbin E. Meacham**[1], **Jennifer L. Ricks**[1], **Hai Jiang**[1], **Douglas A. Lauffenburger**[1,2], and **Michael T. Hemann**[1]

[1]The Koch Institute for Integrative Cancer Research at MIT, Cambridge, MA 02139

[2]Department of Biological Engineering, Massachusetts Institute of Technology, Cambridge, MA 02139

Abstract

The Bcl-2 family encompasses a diverse set of apoptotic regulators that are dynamically activated in response various cell intrinsic and extrinsic stimuli. An extensive variety of cell culture experiments have identified effects of growth factors, cytokines and drugs on BCL-2 family functions, but in vivo studies have tended to focus on role of one or two particular members in development and organ homeostasis. Thus, the ability of physiologically relevant contexts to modulate canonical dependencies that are likely to be more complex has yet to be investigated systematically. In this study, we report findings derived from a pool-based shRNA assay that systematically and comprehensively interrogated the functional dependence of leukemia and lymphoma cells upon various BCL-2 family members across many diverse in vitro and in vivo settings. This approach permitted us to report the first *in vivo* loss of function screen for modifiers of the response to a frontline chemotherapeutic agent. Notably, our results reveal an unexpected role for the extrinsic death pathway as a tissue-specific modifier of therapeutic response. In particular, our findings demonstrate that particular tissue sites of tumor dissemination play critical roles in demarcating the nature and extent of cancer cell vulnerabilities and mechanisms of chemoresistance.

Keywords

Bcl-2 family; mouse models; chemotherapy; in vivo screening; microenvironment

Introduction

Chemotherapy represents a major treatment modality for cancer, and numerous genetic screens have probed the mechanisms underlying cell-intrinsic resistance or sensitivity to front-line chemotherapy (1–6). However, these studies, while informative, have not been adapted to relevant tumor microenvironments, which may contain diverse stromal and/or immune cell types, are subject to immune surveillance, and harbor physical barriers to drug delivery (7). Additionally, the native tumor microenvironment comprises a diverse mixture of chemokines and cytokines that may impact responses to genotoxic agents (8, 9). Thus, the central determinants of therapeutic outcome may be highly dependent upon paracrine survival or stress signals. Indeed, it is well documented that gene function and relevance can vary dramatically when compared *in vivo* versus *in vitro* (8, 10). Consequently, studying the

Corresponding author: Michael T. Hemann, MIT, 77 Massachusetts Ave., 76-361B, Cambridge, MA 02139, hemann@mit.edu 617-324-1964.

*These authors contributed equally to this manuscript.

NIH-PA Author Manuscript

NIH-PA Author Manuscript

NIH-PA Author Manuscript

NIH-PA Author Manuscript

NIH-PA Author Manuscript

NIH-PA Author Manuscript

impact of defined genetic alterations on therapeutic response in native tumor microenvironments is critical for effective drug development, personalized cancer regimens, and the rational design of combination therapies.

Recent advances in the development of tractable mouse models of cancer have, for the first time, enabled the examination of complex sets of defined alterations in individual mice. For example, retroviral infection of murine hematopoietic stem cells or primary embryonic hepatocytes with small pools of short hairpin RNAs (shRNAs), followed by adoptive transfer into lethally-irradiated recipient mice, has been used to screen for suppressors of B cell lymphomagenesis or hepatocellular carcinoma (11, 12). Additionally, *ex vivo* manipulation of lymphoma cells followed by transfer into syngeneic recipient mice has permitted the interrogation of thousands of shRNAs for modulators of tumor growth and dissemination (13). These screens provide powerful proofs of principle that diverse alterations can be introduced in chimeric tumor models *in vivo* and that these systems might permit the simultaneous examination of the relevance of a whole set of genes to therapeutic response in relevant physiological contexts.

Front-line cancer therapies generally exert their effects by modulating the proportion of pro- to anti- apoptotic death regulators, most notably members of the Bcl-2 family (14, 15). Thus, we reasoned that interrogating Bcl-2 family functionality might provide a high-resolution focus on a crucial facet of cytotoxic cellular responses to chemotherapy in a variety of distinct settings. Notably, previous studies using recombinant BH3 peptides in reconstituted mitochondrial suspensions have systematically identified cellular states associated with the loss of function of one of the BH3-only Bcl-2 family members, the loss of function of a multi-domain pro-apoptotic Bcl-2 family member, or the enhanced function of an anti-apoptotic family member; these states characterize the potential range of dysregulation that the Bcl-2 family can acquire during tumorigenesis and demarcate central cell fate decisions that are susceptible to therapeutic intervention (16, 17). However, this approach, while quite powerful, does not allow for the comprehensive examination of the role and relevance of individual Bcl-2 family members to cell death following chemotherapy. Here we describe a complementary *in vivo* screening approach that provides a detailed assessment of the role of each Bcl-2 family member in the response to chemotherapy in heterogeneous tumor environments.

Materials and Methods

shRNA generation

shRNAs targeting the Bcl-2 family (18) were designed using Biopredsi from Novartis. shRNAs were cloned into the MLS (19) retroviral vector containing a Mir30 expression cassette under the transcriptional control of the MSCV LTR and coexpressing GFP. Plasmids were verified for mRNA target knockdown using standard qRT-PCR techniques. Western blots were performed to analyze total protein knock down for a subset of Bcl-2 family members. Bim, Bax, and Bak knockdown are shown in Supp. Figures S1A and B. The shRNA library was constructed by evenly pooling individual minipreps of each individual shRNA. This mixture was co-transfected into Phoenix retroviral packaging cells and pooled virus was collected.

Western Blots

SDS-PAGE was performed according to standard protocols, and gels were transferred to PVDF membranes. The antibodies used were as follows; Bid (polyclonal antisera from Honglin Li), BAX (Cell Signaling Technologies #2772), BAK (Upstate #06-536), BIM (Cell Signaling Technologies #C34C5), Caspase 8 (Cell Signaling Technologies #D35G2),

NIH-PA Author Manuscript

NIH-PA Author Manuscript

NIH-PA Author Manuscript

beta-Actin (Cell Signaling Technologies #4967L), and Tubulin (ECM Biosciences #TM1541).

Luminex bead-based assay

Carboxylated Luminex beads were purchased from Mirai biosystems. Probe oligonucleotides comprised of the shRNA anti-sense strand modified with C12-amine were conjugated to the beads using EDC in a pH 4.5 MES hydrate buffer. Coupling efficiency was validated with sense oligonucleotides. 3500 beads were added to a 50μl reaction volume in a 3M Tetra-methyl ammonium chloride (TMAC) buffer to reduce the differences in T_m that accompany differences in GC content. DNA loading concentrations are as indicated (2-200ng per well were added). Blocking oligos that corresponded to the biotinylated PCR product but lacked the sense portion of the shRNA were added at 100-fold molar excess to compete out the dsPCR product and reduce the preferential re-hybridization of the PCR product. Samples were denatured for 3 min at 95°C and hybridized for 30 minutes at 52°C. Streptavidin-PE (Invitrogen)/TMAC was then added to the wells and incubated for 5 minutes at 52°C. All samples were incubated at 52°C to ensure they stayed at equilibrium, and the PMT setting on the Luminex machine was approximately 520 volts (low calibration).

Polymerase Chain Reaction

Three individual 25μl PCR reactions were performed using a 5' primer targeting the constant hairpin loop region and a 3' primer targeting the vector backbone. The PCR buffer was 2x Failsafe Buffer B (Epicentre Biotechnologies) and we ran 35 cycles with an extension time of 1 minute at 72°C and a hybridization temperature of 52°C for 35 seconds. The 3' primer was biotinylated. Pooled PCR product was column purified and resuspended in 36μl water prior to serial dilution and subsequent measurement.

Cell culture

All lymphoma and leukemia cells were isolated directly from tumor-bearing animals and cultured at 5% CO2 at 37°C. *Eμ-Myc p19*$^{ARF-/-}$ cells were isolated and maintained as described (5). B-ALL cells were maintained as described (20). All *in vitro* viral transduction was performed by co-infecting 1 million cells per 10cm plate. Infection efficiency was quantified by flow cytometry for GFP+ cell populations. Infection efficiencies under 50% were utilized to ensure an MOI of approximately one. Pool composition was measured at the beginning of the experiment, as well as following recovery from an LD90 doxorubicin drug dose. Untreated cells that had grown in culture for the duration of the experiment were used as controls. Hairpin 97mer sequences in the Mir30 context were:

shBid-1-
TGCTGTTGACAGTGAGCGCCACAGAAGATTCCATATCAAATAGTGAAGCCACAGAT GTATTTGATATGGAATCTTCTGTGATGCCTACTGCCTCGGA,

shBid-2-
TGCTGTTGACAGTGAGCGCCACAGAAGATTCCATATCAAATAGTGAAGCCACAGAT GTATTTGATATGGAATCTTCTGTGATGCCTACTGCCTCGGA.

shCaspase 8-
TGCTGTTGACAGTGAGCGAAACTATGACGTGAGCAATAAATAGTGAAGCCACAGAT GTATTTATTGCTCACGTCATAGTTCTGCCTACTGCCTCGGA

Background distribution analysis for *in vivo* screening data

454 sequencing data used to determine CV thresholds is available from the GEO database (accession number GSE16090). Coefficients of variation were calculated by dividing the

NIH-PA Author Manuscript

NIH-PA Author Manuscript

NIH-PA Author Manuscript

standard deviation of the fold change in read number (for any hairpin with >4 reads) by the mean of the fold change. To be included in this analysis hairpins had to be present at high enough quantities to have at least 4 reads. Previously validated hit CVs (13) included IL-6, Lyn, Rac2, Twf, and CrkL and were compared to the background distribution by t-test. Cumulative distributions were plotted in Matlab using the dfittool.

In vivo screening

6-week old C57BL/6J mice (Jackson Laboratories) were tail vein injected with 2 million *Eμ-Myc p19*$^{ARF-/-}$ lymphoma cells expressing the 22 shRNAs targeting the Bcl-2 family. Infection was optimized such that each tumor cell expressed a single shRNA. We sampled pool composition before injection, upon the development of a palpable tumor burden, and upon relapse following IP injection of 8mg/kg of doxorubicin. For *in vivo* screen validation, pure populations of cells expressing shRNAs were isolated by GFP sorting using a FACS ARIA cell sorter. 2 million cells transduced with a vector control or specific shRNAs were injected into syngeneic recipient mice. At the presentation of palpable lymphomas, mice were treated with 10mg/kg doxorubicin and disease free survival/tumor free progression were monitored.

Screening analysis

Luminex intensities for serial dilutions of PCR samples from pooled hairpin libraries were compared by calculating a curve fit for a given sample using the equation (Y=a*(1−exp(−b*x)). Sample integrals were then calculated, and these integral scores were compared after subtracting the initial from the final integral score. All independent Luminex runs were normalized to the maximum signal intensity and all runs performed on different days contained internal standards for day-to-day normalization. Scoring shRNAs were identified following a three-step process. First, in order to eliminate a systematic error for depleting hairpins, we transformed all the data by adding the hairpin mean to all *in vivo* measurements. We then applied two filters. The first filter was based upon a comparison of the distribution of a given shRNA with the variation of neutral hairpins. We required our “hits” to have a coefficient of variation that was equal to or less than 0.4. This allowed us to threshold out approximately 80% of neutral hairpins. The second filter was based upon a comparison of treated samples with untreated hairpin samples. To progress to further validation efforts, we required our treated sample to be different at the 0.10 significance level versus untreated controls.

Data analysis

Linear fits were calculated using a least squares algorithm. Sequences were compared for overlap using the local alignment method of Smith-Waterman in the Matlab function localalign.m. Heat maps were generated in Matlab. Kaplan Meier analyses were performed using Graph Pad Prism software.

Results

A bead-based assay for the direct measurement of pooled shRNA representation

The Bcl-2 family consists of 16 pro- and 6 anti-apoptotic proteins that regulate programmed cell death in response to a diverse set of intrinsic and extrinsic death stimuli (21, 22). To assess how these genes modulate chemotherapy-induced cell death across multiple *in vivo* contexts, as well as across diverse *in vitro* conditions in a multiplexed manner, we adapted a validated set of shRNAs targeting all 22 Bcl-2 family members to Luminex bead-based analysis (Figure 1A and (18)). This technology has previously been used to quantify diverse sets of microRNAs in solution with improved accuracy relative to classic microarray

NIH-PA Author Manuscript

NIH-PA Author Manuscript

NIH-PA Author Manuscript

approaches (23). Thus, we reasoned that this approach could be modified to perform reproducible quantification of sub-genome sized shRNA pools.

Briefly, we covalently coupled an amino modified oligonucleotide that is the reverse complement of the unique guide strand section of each shRNA to fluorescently labeled Luminex beads. Our PCR strategy uses a forward primer complementary to the microRNA loop sequence present in all hairpins and a biotinylated reverse primer complementary to the flanking microRNA sequence (Figure 1B). Thus, all shRNA guide strands can be amplified using common primers, and the quantity of individual shRNAs can be visualized with streptavidin-PE after bead hybridization. Notably, this approach is distinct from barcoded shRNA libraries, in which shRNAs are identifiable by a flanking DNA sequence. In this case, we used the unique portion of the shRNA, itself, as the barcode. This allows for multiplexed shRNA quantification in any vector backbone.

As an initial proof-of-principle experiment, we confirmed that each Bcl-2 shRNA could be quantified by Luminex bead hybridization when starting with similar concentrations of dsPCR product (Supp. Figure S2A). Importantly, while each PCR product with a cognate bead was readily detectable, a control probe exhibited no significant signal with any of the 22 shRNAs in the plasmid library. In fact, the average maximum signal for an shRNA present in the pool was approximately 100-fold higher than the control probe signal. While this negative control ruled out any large magnitude non-specific hybridization, we wanted to rule out smaller amounts of cross hybridization as the source of the variation in the maximum fluorescence intensity of the various probes (Supp. Figure S2B). To this end, we noted a strong relationship between probe GC content and maximum signal intensity. Oligonucleotides deviating from this relationship were analyzed for local sequence alignments across the entire shRNA library utilizing the dynamic programming method of Smith-Waterman (24). The variation in the average local alignment bit scores for all “outlier” probes was highly similar (Supp. Figure S2C), indicating that cross-hybridization is an unlikely contributor to overall signal intensity. Thus, oligonucleotide sequences chosen for optimal siRNA performance are well suited for hybridization-based sequence identification.

We next performed mock enrichment experiments in which known concentrations of genomic DNA from single hairpin infected *Eμ-Myc p19*$^{Arf-/-}$ lymphoma cells were combined at distinct ratios (Supp. Figure S2D). These lymphoma cells were derived from a well-established pre-clinical mouse model of Burkitt’s lymphoma and represent a tractable setting to investigate the genetics of therapeutic response (25, 26). Using these cells, we observed a linear and highly reproducible change in measured fluorescence intensity that tightly correlated with the known fold enrichment of the control sample across 8 fold changes in relative DNA abundance.

The BCL-2 family differentially modulates therapeutic response in distinct B-cell tumors

The initial validation of our measurement technology led us to benchmark this approach against an established single shRNA flow cytometry based assay. In this assay, GFP was used as a surrogate marker for the presence of each of 16 distinct Bcl-2 family member shRNAs, and the impact of gene suppression was determined by the relative change in the percent of GFP positive cells following treatment (18). In each case, we examined the effect of Bcl-2 family gene knockdown on the *in vitro* response of *Eμ-Myc p19*$^{Arf-/-}$ lymphoma cells to the front-line chemotherapeutic doxorubicin (Figure 1C). A linear relationship (r^2=0.89) was observed between multiplexed bead-based measurements and single shRNA flow cytometry measurements of shRNA enrichment and depletion following doxorubicin treatment. Thus, a bead hybridization assay can rapidly and accurately measure shRNA pool composition following drug selection.

NIH-PA Author Manuscript

NIH-PA Author Manuscript

NIH-PA Author Manuscript

A key advantage of shRNA pool-based approaches lies in their inherent adaptability to diverse experimental systems and conditions. In order to test the flexibility of our system, we examined the effects of Bcl-2 family member suppression on doxorubicin response in a distinct cell line. In this case, we examined cells derived from a BCR-Abl driven murine model of B cell acute lymphoblastic leukemia (B-ALL) (27). As observed in the Burkitt's lymphoma model, we could identify a robust Bcl-2 family shRNA drug resistance and sensitivity profile in these cells. However, the shRNA signatures were distinct between cell types. The most obvious feature differentiating the two cell lines was the critical role for the BH3-only member Bim in doxorubicin-induced cell death in B-ALL (Figure 1D). Since Bim levels are known to increase in response to environmental but not genotoxic stress, the involvement of Bim in the response to a DNA damaging agent in this context was unexpected. In order to explore the mechanism of Bim induced cell death, we examined Bim levels in p185+ BCR-Abl ALL cells treated with genotoxic agents (doxorubicin and chlorambucil) and a histone deacetylase inhibitor known to promote significant Bim induction (SAHA) in B cell malignancies (28). Notably, protein levels of Bim were induced acutely following treatment with DNA damaging agents in B-ALL cells (Figure1E). These data highlight the potential of pool-based shRNA approaches to identify tumor cell-specific determinants of therapeutic response.

An *in vivo* screen for microenvironment specific modifiers of therapeutic response

A central challenge in the development of effective anti-cancer approaches is to understand the impact of the tumor microenvironment on therapeutic response. To test whether our system could be used to examine cancer therapy *in vivo*, we performed a screen to identify Bcl-2 family members that modulate the response of lymphomas to doxorubicin. Here, all Bcl-2 family shRNAs were simultaneously co-transfected into viral packaging cells to produce a multi-construct viral pool (Figure 2A). The resulting pool was used to infect primary *Eμ-Myc p19*$^{Arf-/-}$ lymphoma cells *ex vivo*, and transduced cells were tail-vein injected into syngeneic recipient mice. A cohort of 8 mice was sacrificed following tumor onset, and a second cohort was treated with 8mg/kg doxorubicin. Following tumor relapse, lymphoma cells were harvested from lymph nodes and the thymus, two common sites of lymphoma manifestation in the *Eμ-Myc* mouse (25), and the relative shRNA content was compared between untreated and treated tumors in these distinct tumor microenvironments.

A striking feature of the resulting data was the mouse-to-mouse variability in hairpin composition following drug treatment. This suggests that the complexity of the *in vivo* microenvironment can substantially influence the measured effect of a relatively neutral shRNA. Further inspection of this variation suggested that a subset of shRNAs exhibited a level of variation comparable to the *in vitro* data while the remainder showed significantly higher fluctuation (Figure 2B). If otherwise neutral hairpins exhibit larger variation in *in vivo* datasets, the size of this variation may represent a meaningful discriminator to focus on hairpins whose effects are large and reproducible enough to overcome this variability. To determine whether such variation is a consistent feature of *in vivo* data sets, we made use of a comprehensive *in vivo* versus *in vitro* shRNA screening data set (13). Indeed, most shRNAs exhibited high mouse-to-mouse CVs *in vivo* (Figure 2C). However, when we focused on shRNAs shown to exert a biological effect in subsequent validation experiments, we saw a significant decrease in shRNA CVs ($p<0.01$). Thus, variation present in this established data set can be used to generate a CV threshold that identifies shRNAs with a high probability of exerting a relevant biological effect. This cutoff was then employed to filter data generated using our Luminex approach (Figure 2D). As a test of the relevance of this variation cutoff to other drug screens, we examined the stochastic variation in the representation of vector control infected *Eμ-Myc* tumor cells following treatment with the microtubule poison vincristine *in vivo*. Here, we transplanted tumor cells into recipient mice

NIH-PA Author Manuscript

NIH-PA Author Manuscript

NIH-PA Author Manuscript

at a defined infection efficiency, as monitored by GFP expression, and examined the variation in the percentage of GFP positive cells in distinct mice following treatment. Importantly, these controls exhibited an *in vivo* CV that was greater than the doxorubicin variation cutoff (Supp. Figures S3A and B), suggesting that the CV threshold established in this study may be broadly applicable to other data sets.

As additional criteria for examining *in vivo* screening data, we required that shRNA target mRNAs be present in untransduced lymphoma cells and that the representation of a "scoring" shRNA be significantly enriched or depleted as a consequence of doxorubicin treatment (see methods). The resulting list of scoring shRNAs included Bcl-2 family members previously described to influence therapeutic response (17) (Figure 2D and Supp. Table S1). For instance, we found that suppression of the BH3-only protein Puma promoted doxorubicin resistance in both the lymph node and thymus compartments, consistent with previous reports examining either B lymphoma cells or thymocytes (26, 29). Thus, this approach can readily identify important regulators of drug-induced cell death.

The extrinsic death pathway is a thymus specific mediator of therapeutic response

Interestingly, in contrast with Puma and other general cell death regulators, we identified the pro-apoptotic Bcl-2 family member Bid as a specific mediator of doxorubicin cytotoxicity in the thymus but not in the lymph nodes. To validate and extend the genetic result in light of this finding, we performed an *in vivo* GFP competition assay in the spleen, bone marrow, peripheral lymph nodes and thymus. In this assay, GFP positivity is used as a surrogate marker for the presence of a Bid shRNA, and the impact of Bid suppression is determined by the relative change in the percent of GFP positive tumor cells. Consistent with the initial screening data, Bid loss impaired lymphoma cell death in the thymic tumor microenvironment, but not other tumor microenvironments (Figure 3A and B). This tissue specificity was not due to the selective expression of these proteins in specific tumor microenvironments, as we observed similar levels of Bid and its upstream regulator Caspase 8 in the tumor-bearing lymph node and thymus (Supp. Figure S4A and B). Notably, Bid is unique among Bcl-2 family members in that it translocates to the mitochondria following extrinsic activation of death receptors (30, 31). Thus, these data are consistent with a mechanism whereby constitutively present Bid is activated following the release of secreted factors or tumor-stromal cell interactions that are specific to the treated thymic microenvironment.

The relevance of Bid to DNA damage-induced death remains a subject of debate (32, 33). To confirm the importance of Bid to doxorubicin-induced cell death *in vivo*, we injected three cohorts of syngeneic mice with *Eu-Myc p19*$^{Arf-/-}$ lymphoma cells expressing one of two validated shRNAs targeting Bid or a vector control. At tumor onset, all mice were treated with 10mg/kg doxorubicin and monitored for tumor regression and relapse. Suppression of Bid resulted in decreased tumor free survival and tumor cell clearance compared to control tumors (Figure 4A). Furthermore, in mice bearing shBid-transduced lymphomas, 50% of the mice showed no tumor free survival while 90% of control mice exhibited a period of tumor free survival. Notably, in the case of the lymphoma cells used in this study, suppression of Bid *in vitro* had minimal effect on lymphoma cell survival following doxorubicin treatment (Figure 4B). Thus, treatment of these tumors in their native microenvironment reveals genetic dependencies that are not present in cultured cells.

These data suggest that activation of components of the extrinsic cell death pathway potentiate chemotherapeutic efficacy in the thymus. To further interrogate the role of death receptor signaling in therapeutic response in this setting, we targeted Caspase 8, the direct activator of Bid by generating hairpins targeting Caspase 8 (Supp. Figure S4C). Suppression of Caspase 8 in transplanted lymphomas phenocopied the effect of Bid silencing as

NIH-PA Author Manuscript

NIH-PA Author Manuscript

NIH-PA Author Manuscript

measured by tumor free survival (Figure 5A), suggesting an upstream induction of death receptor signaling in the thymus following doxorubicin treatment.

Finally, to confirm the specificity of Bid-induced cell death in the thymus relative to whole organism chemotherapeutic response, we examined the effect of Bid suppression on tumor free survival following doxorubicin treatment in athymic mice. Pure populations of either shBid or vector control transduced lymphoma cells were transplanted into surgically thymectomized recipient mice. Upon the presentation of a palpable disease burden, mice were dosed with 10mg/kg of doxorubicin and monitored for tumor-free and overall survival. In this context, chemotherapeutic response was indistinguishable in the presence or absence of Bid (Figure 5B).

Discussion

We have presented a tractable methodology for pooled shRNA screens that can be rapidly adapted to diverse vector systems and gene families. The value of this system is exemplified by the rapid manner in which drug function can be interrogated in multiple cell types *in vitro* and in diverse anatomical contexts *in vivo*. Importantly, while numerous cell culture-based loss of function screens have been performed to identify modulators of therapeutic response, this is the first report to describe an *in vivo* loss of function therapy screen – the relevance of which is apparent in light of the discordant *in vitro* and *in vivo* phenotypes resulting from Bid suppression. While the set of shRNAs probed in this work is restricted to a particular aspect of cell biology, recent advances in bead-based DNA hybridization now permit the simultaneous resolution of as many as 500 distinct oligonucleotides so that multiple facets can be explored simultaneously. We have recently shown that as many as 1000 distinct shRNAs can be introduced into individual mice (13), suggesting that large shRNA libraries can be combined with this technology to probe the impact of myriad genetic lesions in diverse pathophysiological contexts.

In this study we systematically examined shRNAs targeting the entire Bcl-2 family in multiple *in vitro* and *in vivo* settings. In all therapeutic contexts, we identified a specific BH3 “activator” gene essential for mediating the effects of frontline chemotherapy. Biochemical studies have previously defined critical roles for the BH3 only family members Bid, Puma and Bim. Furthermore, the recent development of a Bid, Puma, and Bim triple knockout mouse confirmed the essential role of these proteins in developmentally regulated apoptosis (34). Interestingly, our data suggests that the relevant “activator” protein can vary quite significantly in neoplastic cells. While an “activator” is always necessary for cell death, the cellular environment or driving oncogene can dramatically shift the precise BH3-only family member that is most relevant for therapy-induced apoptosis. This context-dependent relevance of apoptotic regulators may underlie the significant challenge in eradicating disseminated malignancies and highlights the need to understand the relationship between intrinsic and paracrine signals and Bcl-2 family regulation.

An unexpected finding from this work is that while Caspase 8 and Bid are expressed at similar levels in diverse tumor-bearing locations *in vivo*, they are specifically required for drug efficacy in the thymus. Examined in isolation, this result would suggest that the thymus is a pro-death microenvironment. However, previous studies in thymectomized mice have shown that the thymus can exert a net protective effect on tumor cells following doxorubicin treatment (9). This cytoprotective effect is mediated in a paracrine fashion by thymic endothelial cells that secrete multiple pro-survival cytokines in response to DNA damage. Cytokine induction subsequently upregulates BCL-xL and promotes the survival of target tumor cells. Thus, the unique role of death receptor activity in this context may function to counterbalance unchecked survival signaling following cellular stress in the thymic

NIH-PA Author Manuscript

NIH-PA Author Manuscript

NIH-PA Author Manuscript

microenvironment. Notably, however, the precise mechanism of death receptor engagement in this context remains to be determined. Addition of recombinant death receptor ligands, such as FASL, TNF, and TRAIL *in vitro* fails to induce lymphoma cell death. Consequently, the engagement of death receptor signaling, like survival signaling, may require a more complex concerted action of secreted factors and cell-cell or cell-stromal interactions.

Supplementary Material

Refer to Web version on PubMed Central for supplementary material.

Acknowledgments

The authors would like to thank members of the Lauffenburger and Hemann labs for helpful comments and criticisms. We would also like to thank Hai Jiang for important conceptual and technical contributions to this study. M.T.H. is supported by NIH RO1 CA128803 and the Ludwig Foundation. J.R.P. is a Poitras Graduate Fellow, and J.R.P. and C. E. M. are supported by the MIT Department of Biology training grant. L. A. G. is supported by a Ludwig Fellowship. Additional funding was provided by the Integrated Cancer Biology Program grant 1-U54-CA112967 to D.A.L. and M.T.H.

Grant Numbers: NIH RO1 CA128803 (MTH) and NCI 1-U54-CA112967 (MTH and DAL)

References

1. Bartz SR, Zhang Z, Burchard J, Imakura M, Martin M, Palmieri A, et al. Small interfering RNA screens reveal enhanced cisplatin cytotoxicity in tumor cells having both BRCA network and TP53 disruptions. Mol Cell Biol. 2006; 26:9377–86. [PubMed: 17000754]
2. Berns K, Horlings HM, Hennessy BT, Madiredjo M, Hijmans EM, Beelen K, et al. A functional genetic approach identifies the PI3K pathway as a major determinant of trastuzumab resistance in breast cancer. Cancer Cell. 2007; 12:395–402. [PubMed: 17936563]
3. Huang S, Laoukili J, Epping MT, Koster J, Holzel M, Westerman BA, et al. ZNF423 is critically required for retinoic acid-induced differentiation and is a marker of neuroblastoma outcome. Cancer Cell. 2009; 15:328–40. [PubMed: 19345331]
4. Doles J, Hemann MT. Nek4 status differentially alters sensitivity to distinct microtubule poisons. Cancer Res. 2010; 70:1033–41. [PubMed: 20103636]
5. Burgess DJ, Doles J, Zender L, Xue W, Ma B, McCombie WR, et al. Topoisomerase levels determine chemotherapy response in vitro and in vivo. Proc Natl Acad Sci U S A. 2008; 105:9053–8. [PubMed: 18574145]
6. Smogorzewska A, Desetty R, Saito TT, Schlabach M, Lach FP, Sowa ME, et al. A genetic screen identifies FAN1, a Fanconi anemia-associated nuclease necessary for DNA interstrand crosslink repair. Mol Cell. 2010; 39:36–47. [PubMed: 20603073]
7. Sharpless NE, Depinho RA. The mighty mouse: genetically engineered mouse models in cancer drug development. Nat Rev Drug Discov. 2006; 5:741–54. [PubMed: 16915232]
8. Hideshima T, Mitsiades C, Tonon G, Richardson PG, Anderson KC. Understanding multiple myeloma pathogenesis in the bone marrow to identify new therapeutic targets. Nat Rev Cancer. 2007; 7:585–98. [PubMed: 17646864]
9. Gilbert LA, Hemann MT. DNA damage-mediated induction of a chemoresistant niche. Cell. 2010; 143:355–66. [PubMed: 21029859]
10. Nguyen DX, Bos PD, Massague J. Metastasis: from dissemination to organ-specific colonization. Nat Rev Cancer. 2009; 9:274–84. [PubMed: 19308067]
11. Bric A, Miething C, Bialucha CU, Scuoppo C, Zender L, Krasnitz A, et al. Functional identification of tumor-suppressor genes through an in vivo RNA interference screen in a mouse lymphoma model. Cancer Cell. 2009; 16:324–35. [PubMed: 19800577]
12. Zender L, Xue W, Zuber J, Semighini CP, Krasnitz A, Ma B, et al. An oncogenomics-based in vivo RNAi screen identifies tumor suppressors in liver cancer. Cell. 2008; 135:852–64. [PubMed: 19012953]

NIH-PA Author Manuscript

NIH-PA Author Manuscript

NIH-PA Author Manuscript

13. Meacham CE, Ho EE, Dubrovsky E, Gertler FB, Hemann MT. In vivo RNAi screening identifies regulators of actin dynamics as key determinants of lymphoma progression. Nat Genet. 2009; 41:1133–7. [PubMed: 19783987]

14. Adams JM, Cory S. Bcl-2-regulated apoptosis: mechanism and therapeutic potential. Curr Opin Immunol. 2007; 19:488–96. [PubMed: 17629468]

15. Cotter TG. Apoptosis and cancer: the genesis of a research field. Nat Rev Cancer. 2009; 9:501–7. [PubMed: 19550425]

16. Certo M, Del Gaizo Moore V, Nishino M, Wei G, Korsmeyer S, Armstrong SA, et al. Mitochondria primed by death signals determine cellular addiction to antiapoptotic BCL-2 family members. Cancer Cell. 2006; 9:351–65. [PubMed: 16697956]

17. Deng J, Carlson N, Takeyama K, Dal Cin P, Shipp M, Letai A. BH3 profiling identifies three distinct classes of apoptotic blocks to predict response to ABT-737 and conventional chemotherapeutic agents. Cancer Cell. 2007; 12:171–85. [PubMed: 17692808]

18. Jiang H, Pritchard JR, Williams RT, Lauffenburger DA, Hemann MT. A mammalian functional-genetic approach to characterizing cancer therapeutics. Nat Chem Biol. 2011; 7:92–100. [PubMed: 21186347]

19. Dickins RA, Hemann MT, Zilfou JT, Simpson DR, Ibarra I, Hannon GJ, et al. Probing tumor phenotypes using stable and regulated synthetic microRNA precursors. Nat Genet. 2005; 37:1289–95. [PubMed: 16200064]

20. Williams RT, den Besten W, Sherr CJ. Cytokine-dependent imatinib resistance in mouse BCR-ABL+, Arf-null lymphoblastic leukemia. Genes Dev. 2007; 21:2283–7. [PubMed: 17761812]

21. Letai AG. Diagnosing and exploiting cancer's addiction to blocks in apoptosis. Nat Rev Cancer. 2008; 8:121–32. [PubMed: 18202696]

22. Youle RJ, Strasser A. The BCL-2 protein family: opposing activities that mediate cell death. Nat Rev Mol Cell Biol. 2008; 9:47–59. [PubMed: 18097445]

23. Lu J, Getz G, Miska EA, Alvarez-Saavedra E, Lamb J, Peck D, et al. MicroRNA expression profiles classify human cancers. Nature. 2005; 435:834–8. [PubMed: 15944708]

24. Smith TF, Waterman MS. Identification of common molecular subsequences. J Mol Biol. 1981; 147:195–7. [PubMed: 7265238]

25. Adams JM, Harris AW, Pinkert CA, Corcoran LM, Alexander WS, Cory S, et al. The c-myc oncogene driven by immunoglobulin enhancers induces lymphoid malignancy in transgenic mice. Nature. 1985; 318:533–8. [PubMed: 3906410]

26. Jiang H, Reinhardt HC, Bartkova J, Tommiska J, Blomqvist C, Nevanlinna H, et al. The combined status of ATM and p53 link tumor development with therapeutic response. Genes Dev. 2009; 23:1895–909. [PubMed: 19608766]

27. Williams RT, Roussel MF, Sherr CJ. Arf gene loss enhances oncogenicity and limits imatinib response in mouse models of Bcr-Abl-induced acute lymphoblastic leukemia. Proc Natl Acad Sci U S A. 2006; 103:6688–93. [PubMed: 16618932]

28. Lindemann RK, Newbold A, Whitecross KF, Cluse LA, Frew AJ, Ellis L, et al. Analysis of the apoptotic and therapeutic activities of histone deacetylase inhibitors by using a mouse model of B cell lymphoma. Proceedings of the National Academy of Sciences of the United States of America. 2007; 104:8071–6. [PubMed: 17470784]

29. Villunger A, Michalak EM, Coultas L, Mullauer F, Bock G, Ausserlechner MJ, et al. p53- and drug-induced apoptotic responses mediated by BH3-only proteins puma and noxa. Science. 2003; 302:1036–8. [PubMed: 14500851]

30. Wang K, Yin XM, Chao DT, Milliman CL, Korsmeyer SJ. BID: a novel BH3 domain-only death agonist. Genes Dev. 1996; 10:2859–69. [PubMed: 8918887]

31. Li H, Zhu H, Xu CJ, Yuan J. Cleavage of BID by caspase 8 mediates the mitochondrial damage in the Fas pathway of apoptosis. Cell. 1998; 94:491–501. [PubMed: 9727492]

32. Zinkel SS, Hurov KE, Ong C, Abtahi FM, Gross A, Korsmeyer SJ. A role for proapoptotic BID in the DNA-damage response. Cell. 2005; 122:579–91. [PubMed: 16122425]

33. Kaufmann T, Tai L, Ekert PG, Huang DC, Norris F, Lindemann RK, et al. The BH3-only protein bid is dispensable for DNA damage- and replicative stress-induced apoptosis or cell-cycle arrest. Cell. 2007; 129:423–33. [PubMed: 17448999]

NIH-PA Author Manuscript

NIH-PA Author Manuscript

NIH-PA Author Manuscript

34. Ren D, Tu HC, Kim H, Wang GX, Bean GR, Takeuchi O, et al. BID, BIM, and PUMA are essential for activation of the BAX- and BAK-dependent cell death program. Science. 2010; 330:1390–3. [PubMed: 21127253]

NIH-PA Author Manuscript

NIH-PA Author Manuscript

NIH-PA Author Manuscript

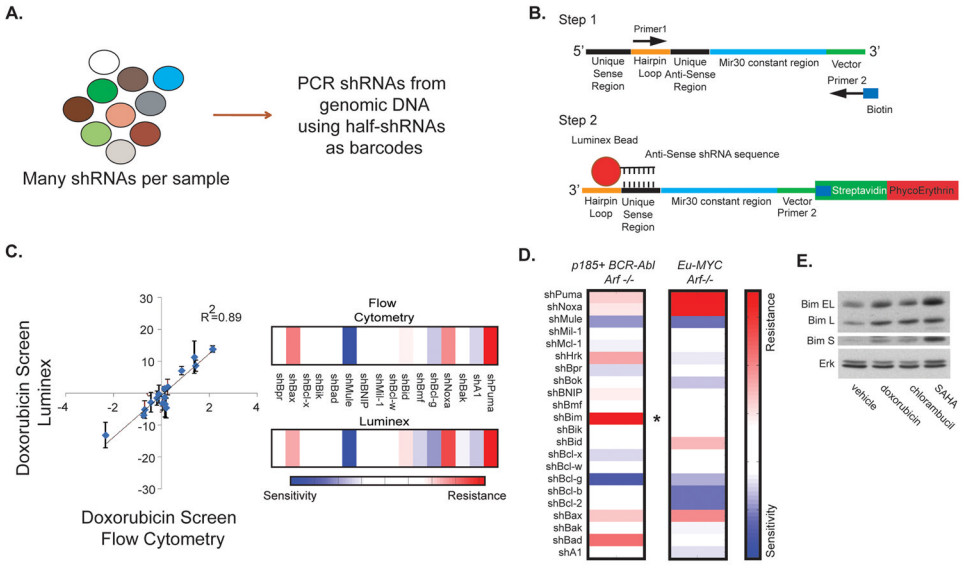

Figure 1. Examining the role of the entire Bcl-2 family in therapeutic response

(A) A schematic depicting the difference between single and pool-based evaluation of shRNA composition**. (B)** A diagram illustrating the Luminex-based shRNA PCR strategy. PCR primers were designed from constant regions flanking all hairpins. After PCR amplification, a biotinylated primer is used to measure hairpin abundance, and the unique fluorescence of the luminex bead distinguishes hairpin identity. **(C)** A comparison of the bead-based quantification of hairpin representation following doxorubicin treatment with single cell flow cytometry measurements (18). (Left) Bead-based measurements are plotted against each corresponding single hairpin measurements. (Right) Heat maps comparing shRNA enrichment and depletion using bead-based and flow cytometry approaches. **(D)** A heat map comparing the impact of depleting each Bcl-2 family hairpin on the response to doxorubicin treatment in *Eμ-MYC p19*$^{Arf-/-}$ lymphomas and *p185 BCR-Abl+ p19*$^{Arf-/-}$ B-ALLs. The asterisk demarcates the differential impact of suppressing the BH3-only protein Bim on doxorubicin sensitivity in these two cell types. **(E)** *p185 BCR-Abl+ p19*$^{Arf-/-}$ cells were treated for 12 hrs at an LD90 of the indicated compounds and analyzed for Bim levels by western blot.

NIH-PA Author Manuscript

NIH-PA Author Manuscript

NIH-PA Author Manuscript

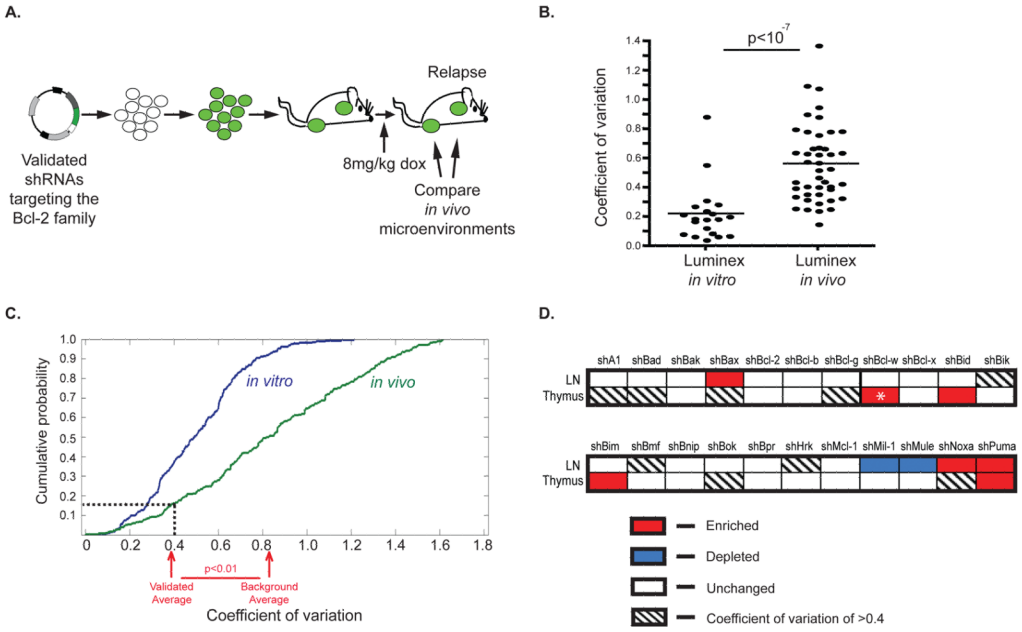

Figure 2. An *in vivo* shRNA screen for modulators of doxorubicin response

(A) A diagram depicting the *in vivo* screening strategy. Pooled shRNAs targeting Bcl-2 family members were retrovirally transduced into *Eμ-MYC p19*$^{Arf-/-}$ lymphomas. shRNA composition was measured either following the presentation of palpable tumor burden or following tumor relapse after treatment with 8mg/kg doxorubicin. **(B)** A comparison of the coefficient of variation (CV) for hairpins targeting the Bcl-2 family in cell culture versus *in vivo* screens using a Luminex measurement methodology. **(C)** An analysis of the distribution of shRNA CV values for a large *in vitro* versus *in vivo* screening data set generated by high-throughput sequencing. The vertical line represents the CV threshold used to filter *in vivo* data. The arrows denote averages for validated hairpins relative to all hairpins **(D)** Bcl-2 family "hits" following filtering for CV and enrichment criteria and separated by anatomical niche. The asterisk denotes a Bcl-w shRNA that scored as enriched in the thymus, but was excluded due to the lack of Bcl-w expression in this context.

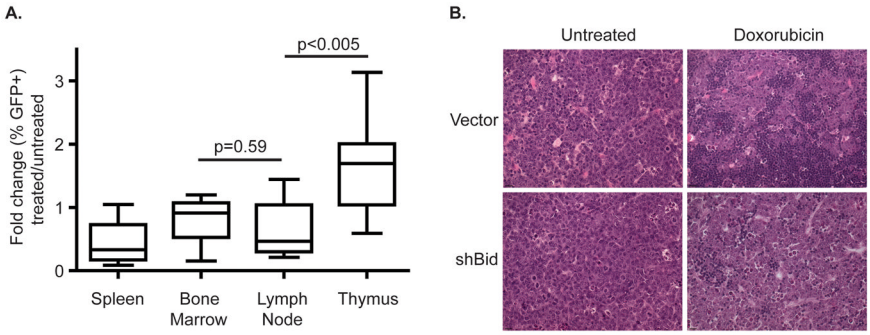

Figure 3. Bid potentiates doxorubicin efficacy in the thymus

(A) A graph depicting an *in vivo* GFP competition assay in lymphoma cells partially transduced with shBid-1. Mice were injected with partially transduced lymphoma populations. At tumor onset all mice were treated with 10mg/kg doxorubicin. 72 hours after treatment, mice were sacrificed and surviving lymphoma populations were harvested. Fold change in GFP percentage was assessed 48 hours later (n≥4). **(B)** H&E stained sections from mice bearing vector control or shBid thymic lymphomas. Mice were treated with 10mg/kg doxorubicin and sacrificed 48 hours later. Representative fields from treated and untreated are shown at 25x magnification. Dark patches in treated vector control tumors indicate sites of normal lymphocyte infiltration.

NIH-PA Author Manuscript NIH-PA Author Manuscript NIH-PA Author Manuscript

NIH-PA Author Manuscript
NIH-PA Author Manuscript
NIH-PA Author Manuscript

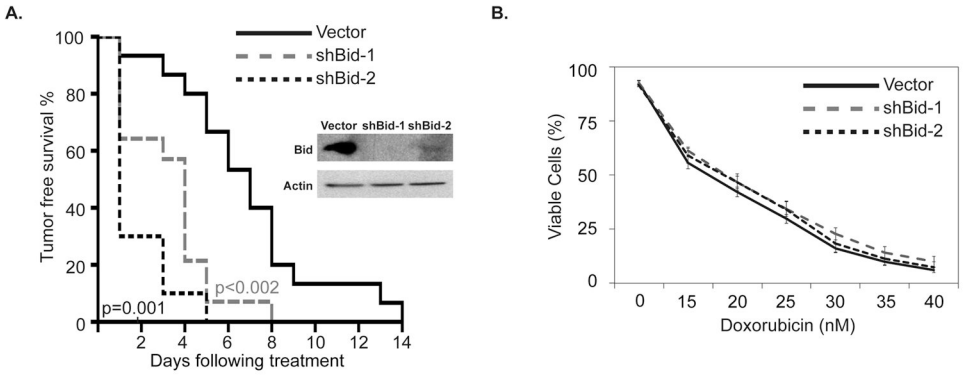

Figure 4. Bid status affects therapeutic outcome *in vivo*, but not *in vitro*

(A) A Kaplan-Meier curve showing tumor free survival in mice bearing vector or shBid lymphomas. All mice were treated with a single dose of 10mg/kg doxorubicin (n≥10). (Inset) A western blot showing Bid protein levels in the presence of Bid shRNAs. **(B)** A dose response curve showing the relative viability of lymphoma cells treated with doxorubicin *in vitro* for 48 hours. Lymphoma cells were transduced with either a vector control or an shRNA targeting Bid.

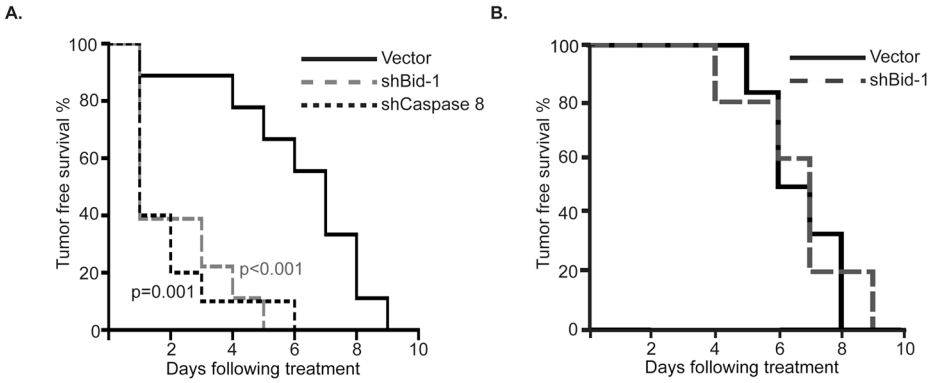

Figure 5. The extrinsic death pathway mediates doxorubicin response in the thymusx

(A) A Kaplan-Meier curve showing tumor free survival of mice bearing vector, shBid or shCaspase 8 expressing lymphomas. All mice were treated with a single dose of 10mg/kg doxorubicin (n≥10). **(B)** A Kaplan-Meier curve showing the tumor free survival of thymectomized mice transplanted with pure populations of lymphoma cells transduced with shBid or a vector control. All mice were treated with a single dose of 10mg/kg doxorubicin (n=6 for both cohorts).

NIH-PA Author Manuscript NIH-PA Author Manuscript NIH-PA Author Manuscript